乱流の減衰過程に及ぼす高分子の影響 (多重物理・多重スケール乱流現象の数理)

AUTHOR(S):

WATANABE, Takeshi; GOTOH, Toshiyuki

CITATION:

WATANABE, Takeshi ...[et al]. 乱流の減衰過程に及ぼす高分子の影響 (多重物理・多重スケール乱流現象の数理). 数理解析研究所講究録 2014, 1882: 55-64

ISSUE DATE:

2014-04

URL:

http://hdl.handle.net/2433/195663

数理解析研究所講究録
第1882巻 2014年 55-64

乱流の減衰過程に及ぼす高分子の影響

名古屋工業大学大学院・創成シミュレーション工学専攻
渡邊 威 (Takeshi WATANABE) watanabe@nitech.ac.jp
後藤 俊幸 (Toshiyuki GOTOH) gotoh.toshiyuki@nitech.ac.jp
Department of Scientific and Engineering Simulation, Nagoya Institute of Technology

Abstract

Nature of decaying turbulence of the dilute polymer solution is numerically investigated by using the hybrid Eulerian-Lagrangian simulations with making full use of the large-scale parallel computation. When the Weissenberg number W_i was increased, we observed the power-law decay of the kinetic energy and pressure spectra as $E(k) \sim k^{-\alpha}$ and $E_p(k) \sim k^{-\beta}$ in the range below the Kolmogorov length l_K when the turbulence adequately decayed. The exponents α and β were respectively $\alpha = 4.2 - 4.6$ and $\beta = 2.8 - 3.2$, and decreased with an increase of W_i. It was found that the probability density functions for the longitudinal velocity derivative and pressure fields were respectively close to the Gaussian irrespective of W_i. We discuss the relationship between the present results and the previous experimental and numerical studies for the elastic turbulence which is characterized by the larger W_i and the Reynolds number is below unity.

Polymer solution flow characterized by both a Reynolds number (Re) less than unity and higher elasticity indicates irregular fluctuations in space and time. This phenomenon is referred to as elastic turbulence [1], and has been investigated with great interest [2, 3, 4, 5, 6, 7, 8, 9]. One of the remarkable natures of elastic turbulence is that the kinetic energy spectrum $E(k)$ obeys the power-law form as $E(k) \sim k^{-\alpha}$ with $\alpha = 3.5$ in experiment [1] and with $\alpha = 3.8$ in the direct numerical simulation (DNS) of the Oldroyd-B model under a two-dimensional Kolmogorov flow [6, 7]. Another interesting property of elastic turbulence is represented by non-Gaussian statistics of velocity derivatives field similar to the case for high-Reynolds number Newtonian turbulent flow [8]. Recent experimental study also indicates that the pressure spectrum $E_p(k)$ also shows the power-law decay $E_p(k) \sim k^{-\beta}$ with a exponent β being close to 3, and pressure fluctuations are strongly non-Gaussian [9]. All above results indicate that the polymer solution flow becomes turbulent state in spite of $Re = O(1)$, and the statistical nature of it is similar to that obtained by the turbulent flows for the Newtonian fluid.

In a previous study [10], we developed a simulation method for the dilute polymer solution flows by using hybrid approach, in which a Brownian dynamics simulation (BDS) for a huge number of dumbbell model ($O(10^{10})$) coupled with a DNS of turbulent flow was performed using large-scale parallel computations. We examined the modification of the decaying turbulence for various polymer concentration and Weissenberg number, $W_i = \tau/\tau_K$, which is the ratio of the polymer relaxation time τ to the Kolmogorov time $\tau_K \equiv (\nu_s/\varepsilon)^{1/2}$ for the smallest eddy in turbulence (ν_s and ε are respectively the kinematic viscosity of the solvent fluid and the average rate of the energy dissipation of turbulence).

One of the most remarkable results reported in [10] is the fact that when the turbulence adequately decays and $W_i > 1$ the kinetic energy spectrum obeys the power-law decay of $E(k,t) \sim k^{-\alpha}$ with $\alpha = 4.7$ at wavenumbers higher than the Kolmogorov wavenumber

$1/l_K \equiv (\varepsilon/\nu_s^3)^{1/4}$. The value of $\alpha = 4.7$ is considerably larger than the exponents obtained for elastic turbulence as mentioned above, although this result is consistent with the theoretical prediction using the simplified viscoelastic model, where the scaling exponent α must be greater than 3 [11]. We progressed our study by performing the additional simulations with larger W_i values, and found that the value of α decreased when W_i was increased [12]. However the case by largest W_i run in [12] (corresponding to Run D3 in this study) gave the value $\alpha = 4.19$, which remains slightly larger than those by previous studies. Thus the understanding on the relationship between our numerical results and the elastic turbulence is insufficient at present.

In this study, we develop the previous study [12] by performing the more detailed analyses. We examine the scaling behavior of the pressure spectrum, in addition to the kinetic energy spectrum, in isotropic decaying turbulence with polymer additives by computing the larger W_i case than those in [12]. We focus our interest on the power-law behavior of these spectra and their W_i-dependences. Moreover we investigate the behavior of probability density function (PDF) for velocity derivative and pressure field fluctuations when the power-law spectrum is observed. Then the similarity and disparity between the present numerical results and those by elastic turbulence are discussed.

The long-chain polymer is modeled by the two-beads connected by the nonlinear spring, so called dumbbell model [13]. The governing equations of motion for the n-th dumbbell is given by

$$\frac{d\boldsymbol{R}^{(n)}}{dt} = \boldsymbol{u}_1^{(n)} - \boldsymbol{u}_2^{(n)} - \frac{1}{2\tau} f\left(\frac{|\boldsymbol{R}^{(n)}|}{L_{max}}\right)\boldsymbol{R}^{(n)} + \frac{r_{eq}}{\sqrt{2\tau}}\left(\boldsymbol{W}_1^{(n)} - \boldsymbol{W}_2^{(n)}\right), \tag{1}$$

$$\frac{d\boldsymbol{r}_g^{(n)}}{dt} = \frac{1}{2}\left(\boldsymbol{u}_1^{(n)} + \boldsymbol{u}_2^{(n)}\right) + \frac{r_{eq}}{\sqrt{8\tau}}\left(\boldsymbol{W}_1^{(n)} + \boldsymbol{W}_2^{(n)}\right), \quad \boldsymbol{u}_\alpha^{(n)} \equiv \boldsymbol{u}(\boldsymbol{x}_\alpha^{(n)}(t), t), \tag{2}$$

where $\boldsymbol{R}^{(n)}(t)$ and $\boldsymbol{r}_g^{(n)}(t)$ are, respectively, the end-to-end vector and the center-of-mass vector of the n-th dumbbell. We adopt the finitely extensible nonlinear elastic (FENE) model $f(z) = 1/(1-z^2)$ for the elastic force of a dumbbell [13, 14]. In Eq.(1), L_{max} is the maximum extension length of the dumbbell because $f(z \to 1) = \infty$. The term $\boldsymbol{W}_{1,2}^{(n)}(t)$ indicates a random force representing the Brownian motion of particles in the solvent fluid, which obeys Gaussian statistics with a white-in-time correlation of

$$\langle W_{\alpha,i}^{(n)}(t)\rangle = 0, \tag{3}$$

$$\langle W_{\alpha,i}^{(n)}(t) W_{\beta,j}^{(m)}(s)\rangle = \delta_{\alpha\beta}\delta_{ij}\delta_{nm}\delta(t-s), \tag{4}$$

where $\langle\cdots\rangle$ denotes the ensemble average. The subscripts α, β, i, j, n, and m take the values $(\alpha,\beta) = 1$ or 2, $(i,j) = 1$, 2, and 3, and $(n,m) = 1, 2, \cdots, N_t$, respectively. Moreover, δ_{ij} denotes the Kronecker delta, and $\delta(t)$ is the Dirac delta function. The constants $\tau \equiv \zeta/4k$ and $r_{eq} \equiv \sqrt{k_B T/k}$ are, respectively, the relaxation time and the equilibrium length of the dumbbell under $\boldsymbol{u}(\boldsymbol{x},t) = \boldsymbol{0}$. Here, k is the spring constant, and $\zeta \equiv 6\pi\nu_s\rho_s a$ (ρ_s is the density of the solvent fluid and a is the bead radius). Also, k_B and T are the Boltzmann constant and temperature, respectively.

The turbulent velocity field obeys the continuity equation for an incompressible fluid and the Navier-Stokes (NS) equations

$$\nabla \cdot \boldsymbol{u} = 0, \quad \frac{\partial \boldsymbol{u}}{\partial t} + \boldsymbol{u} \cdot \nabla \boldsymbol{u} = -\nabla p + \nu_s \nabla^2 \boldsymbol{u} + \nabla : \boldsymbol{T}^p, \tag{5}$$

where $p(\boldsymbol{x}, t)$ is the pressure field. Here, ρ_s is set to unity and is equal to the density of bead ρ_p representing the polymer. The polymer stress tensor $\boldsymbol{T}^p(\boldsymbol{x}, t)$ due to the force acting on the fluid from the dispersed dumbbells is defined by

$$T^p_{ij}(\boldsymbol{x}, t) = \frac{\nu_s \eta}{\tau} \left(\frac{L^3_{box}}{N_t} \right) \sum_{n=1}^{N_t} \left[\frac{R^{(n)}_i R^{(n)}_j}{r^2_{eq}} f\left(\frac{|\boldsymbol{R}^{(n)}|}{L_{max}} \right) - \delta_{ij} \right] \delta(\boldsymbol{x} - \boldsymbol{r}^{(n)}_g), \tag{6}$$

where N_t is the total number of polymers required to realize the experimental situation, $\eta \equiv (3r_{eq}/4a)^2 \Phi_V$ is the zero-shear viscosity ratio of the polymer ν_p to the solution viscosity ($\eta = \nu_p/\nu_s$), and $\Phi_V \equiv (8\pi N_t/3)(a/L_{box})^3$ represents the volume fraction of the ensemble of dumbbells.

The numerical simulations of Eqs.(1) through (6) are performed in a periodic box with periodicity $L_{box} = 2\pi$ using the pseudo-spectral method in space and the second-order Runge–Kutta method in time. A total of 128^3 grid points are used to solve the NS equations. The total number of dumbbells in computation is $N_{comp} = N_t/b = 5.04 \times 10^8$ for all runs presented in this paper, where b is the artificial parameter representing the number of *replica* dumbbells. This reduces the computational cost of the computation of $N_t = O(10^{13})$ dumbbells [10]. Here we set $b = 9 \times 10^4$, giving the values $\Phi_V = 1.01 \times 10^{-4}$ and $\eta = 0.1045$, respectively.

The initial velocity field is given by the random solenoidal field obeying Gaussian statistics, with an energy spectrum

$$E(k, 0) = 16\sqrt{\frac{2}{\pi}} \left(\frac{u_0^2}{k_0} \right) \left(\frac{k}{k_0} \right)^4 \exp\left(-2 \left(\frac{k}{k_0} \right)^2 \right). \tag{7}$$

We set $u_0 = 1$ and $k_0 = 2$, yielding the initial value of the Taylor micro-scale Reynolds number $R_\lambda(0) = 52$. The dumbbells are uniformly and randomly distributed over the computational domain. The initial configuration of each dumbbell is set according to $\boldsymbol{R}^{(n)}(0) = \sqrt{3} r_{eq} \hat{\boldsymbol{n}}^{(n)}$, where $\hat{\boldsymbol{n}}^{(n)}$ is a random unit vector, which is isotropically distributed.

Parallel computations are performed in order to evaluate the convection and deformation of the dispersed dumbbells. The program is parallelized using Message Passing Interface (MPI). The details on the parallelized method can be found in [12]. The fluid velocity at the bead position is interpolated using the TS13 scheme [15]. Since the center-of-mass vector $\boldsymbol{r}^{(n)}_g$ for each of the dumbbells is not on the grid points for the DNS computation, we need an approximate expression when computing the polymer stress term (6). The delta function in (6) is approximated by the weight function $\delta_\Delta(\boldsymbol{x} - \boldsymbol{r}^{(n)}_g)$ used for the tri-linear interpolation scheme [16]. The other parameter settings are described in detail in [10].

We examine five cases of decaying turbulence for several values of W_i while fixing the other parameters. One of them is performed without polymers (one-way coupling, named as Run A). The values of the typical numerical parameters are listed in table 1.

Table 1: Parameters for the hybrid simulations of decaying turbulence and Brownian dynamics for dispersed dumbbells. The values of τ listed below are determined using the values of W_i given in the table and the minimum value of $\tau_K(t)$ during the simulation without the polymer additives (one-way coupling simulation).

	τ	$R_\lambda(t^* = 20)$	W_i^{peak}	$W_i(t^* = 20)$
Run A	–	10.38	–	–
Run D1	4.903	3.525	25	1.655
Run D2	9.806	3.206	50	3.842
Run D3	19.612	3.065	100	7.470
Run D4	39.227	3.028	200	13.32

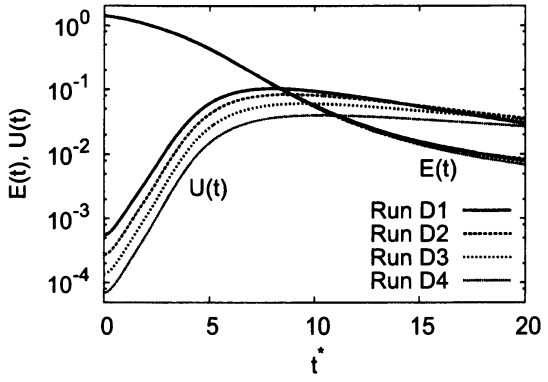

Figure 1: Comparison of the temporal evolutions of the kinetic energy of fluid motion $E(t)$ and the potential energy for the ensemble of dumbbells $U(t)$ for Runs D1, D2, D3, and D4.

Figure 1 shows the temporal evolution of the average kinetic energy of fluid motion $E(t)$ and of the potential energy for the ensemble of dumbbells $U(t)$, which are defined as follows:

$$E(t) = \frac{1}{2}\langle \boldsymbol{u}(\boldsymbol{x}, t)^2 \rangle_V \tag{8}$$

and

$$U(t) = -\frac{\nu_s \eta}{2\tau}\left(\frac{L_{max}}{r_{eq}}\right)^2 \frac{1}{N_{comp}} \sum_{n=1}^{N_{comp}} \ln\left[1 - \left(\frac{|\boldsymbol{R}^{(n)}(t)|}{L_{max}}\right)^2\right] \tag{9}$$

for all of the runs, respectively, where $\langle \cdots \rangle_V$ represents the volume average over the computational domain $V = L_{box}^3$. Hereinafter, figures are plotted using non-dimensional time $t^* \equiv k_0 u_0 t$. The kinetic energy $E(t)$ decays monotonically with time, and the curves collapse onto a single curve irrespective of W_i. The values of $E(t)$ at the end of the simulations are much smaller than their initial values, meaning that the turbulence adequately decayed at $t^* = 20$. On the other hand, $U(t)$ increases with time for $t^* < 7$, which indicates that the turbulence kinetic energy is transferred to the potential energy of the ensemble of dumbbells in addition to the heat. Moreover, $U(t)$ starts to decay at around $t^* = 7$, indicating that the portion of restored potential energy is also back-transferred to turbulence and is dissipated due to the viscosity. Note that $U(t)$ is larger than $E(t)$ in the range of $t^* > 11$ for all of the runs.

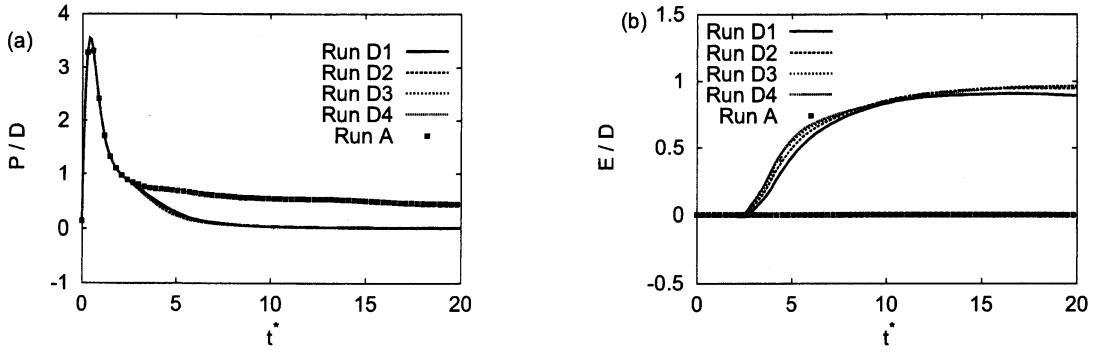

Figure 2: Comparison of the temporal evolutions of (a) the mean enstrophy production rate (S) divided by the mean enstrophy dissipation rate (D) and of (b) the mean enstrophy production/inhibition rate due to polymer additives (P) divided by the mean enstrophy dissipation rate for Runs D1,D2,D3, and D4. Run A is due to the one-way coupling case.

Because the kinetic energy decays with time, the Reynolds number

$$R_\lambda(t) = \sqrt{\frac{20}{3\nu_s\varepsilon(t)}}E(t), \tag{10}$$

where $\varepsilon(t) = \nu_s\langle(\nabla \boldsymbol{u})^2\rangle_V$ is the mean dissipation rate of the kinetic energy, also decays with time [12]. The typical values of $R_\lambda(t)$ at $t^* = 20$ are listed in table 1. We clearly confirm that R_λ is order unity when $t^* = 20$. In contrast, the local Weissenberg number $W_i(t) = \tau/\tau_K(t)$ becomes larger than unity for all of the runs when $t^* = 20$ as shown in table 1, and increase with τ. Thus at the end of simulation a state characterized by $R_\lambda = O(1)$ and $W_i \gg 1$, close to the situation of elastic turbulence, is achieved. We note that the coil-stretch transition of long-chain polymers occurs when $W_i = 3 - 4$ [17].

The enstrophy is defined by the mean squared vorticity as $E_\omega(t) = \langle\boldsymbol{\omega}^2\rangle_V/2$ with $\boldsymbol{\omega} = \nabla \times \boldsymbol{u}$. The transport equation of $E_\omega(t)$ is derived from the NS equations as

$$\frac{d}{dt}E_\omega(t) = \langle\boldsymbol{\omega}\cdot(\boldsymbol{\omega}\cdot\nabla\boldsymbol{u})\rangle_V + \langle(\nabla\times\boldsymbol{\omega})\cdot(\nabla:\boldsymbol{T}^p)\rangle_V - \nu\langle(\nabla\boldsymbol{\omega})^2\rangle_V. \tag{11}$$

The terms on the right hand side (R.H.S.) of Eq.(11) are the mean enstrophy production, mean enstrophy exchanges due to polymers, and the mean enstrophy dissipation rate, respectively (named P, E, and D in order). Figure 2 shows the temporal evolutions of (a) the mean enstrophy production (P) and of (b) the mean enstrophy exchanges due to polymers (E), divided by the enstrophy dissipation rate (D). These indicate that the contribution of term P to the production of enstrophy is almost negligible for $t^* > 10$, while the term E shows the positive finite values in this range. This clearly represents the fact that the vorticity stretching term has an negligible influence on producing the turbulent fluctuations, and the turbulent state is kept by the term E which is originated from the strong coupling between the vorticity and stretching dumbbells. When we consider the Newtonian case (Run A), the term P balances to the enstrophy dissipation, so that the vorticity stretching is the crucial mechanism for keeping the turbulent state in the decay regime. On the other hand the

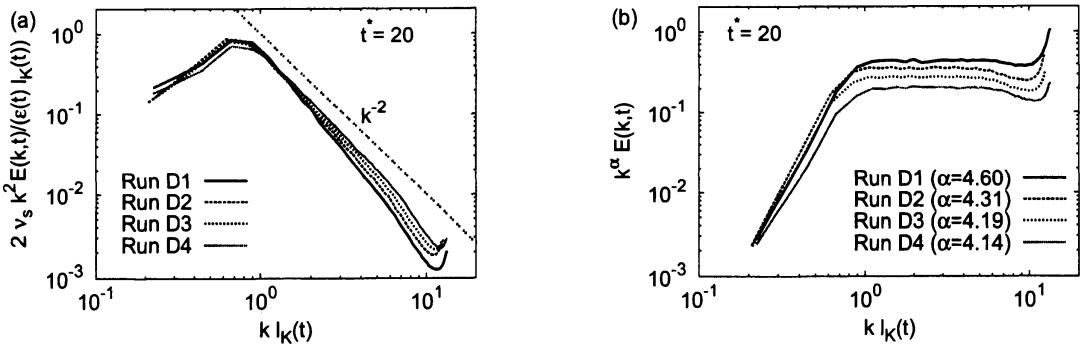

Figure 3: Comparison of the kinetic energy spectra $E(k,t)$ by (a) normalized plot of dissipation spectra using Kolmogorov scaling and by (b) compensated plot by multiplying k^α obtained at $t^* = 20$ for Runs D1, D2, D3, and D4. Scaling exponent α for each runs is evaluated by the least square fitting in the range $2 \leq kl_K(t) \leq 5$.

decay of polymer solution turbulent flow is maintained due to the stronger elasticity which is originated from the elastic energy restored in the decay regime of turbulence ($t^* < 10$).

Figures 1 and 2 suggest that the mechanism of turbulence decay for polymer laden flow is quite different from the case of turbulence for Newtonian fluid. Decaying process of turbulence is categorized into three stages as follows:

$s1$) Turbulence develops from its initial value at the time that the mean energy dissipation reaches its maximum value. Then the dumbbells are rapidly stretched by turbulence, increasing $U(t)$.

$s2$) Turbulence starts to decay by the actions of viscosity and energy transfer to the ensemble of dumbbells, while the dumbbells remain stretching up to the time $E(t) \sim U(t)$.

$s3$) The restored potential energy $U(t)$ decays with time with the rate slower than $E(t)$, meaning that the back transfer of energy from the ensemble of dumbbells to turbulence occurs.

In the stage $s1$) the energy transfer from turbulence to ensemble of dumbbells is active, while the flow field is maintained by the back energy transfer from the ensemble of dumbbells in the stage $s3$). The turbulence statistics in stage $s3$) is thus governed by the elastic nature of polymers, meaning that the situation is quite similar to the case of elastic turbulence.

Next we investigate the scaling behavior of kinetic energy spectrum $E(k,t)$ obtained at $t^* = 20$. The spectrum $E(k,t)$ is defined by

$$E(k,t) = 2\pi k^2 \langle |\hat{\boldsymbol{u}}(\boldsymbol{k},t)|^2 \rangle_s \tag{12}$$

in terms of the Fourier amplitude $\hat{\boldsymbol{u}}(\boldsymbol{k},t)$ where $\langle \cdots \rangle_s$ is the average taken over the spherical shell within $k - \Delta k/2 < |\boldsymbol{k}| \leq k + \Delta k/2$ in the wavenumber space. Figure 3 (a) compares the kinetic energy spectra obtained for all of the runs, where we plot the dimensionless form of dissipation spectra $\hat{D}(kl_K(t),t)$ defined using the Kolmogorov scaling as

$$\hat{D}(kl_K(t),t) = \frac{2\nu_s k^2 E(k,t)}{\varepsilon(t) l_K(t)}, \tag{13}$$

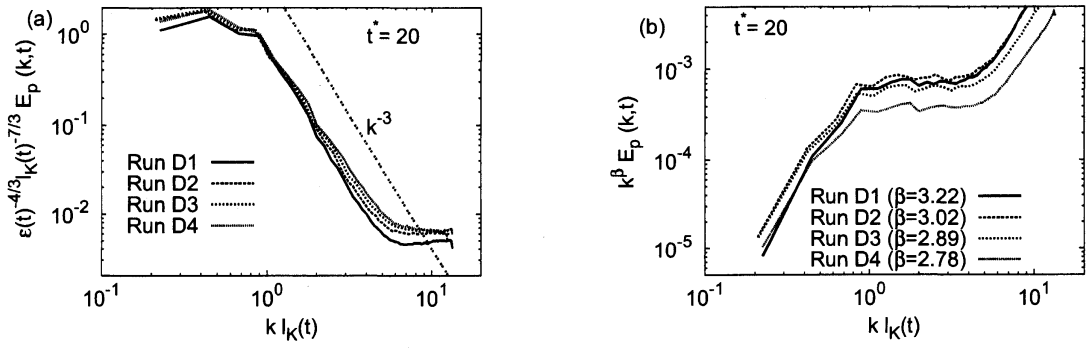

Figure 4: Comparison of the pressure spectra for (a) normalized plot using the Kolmogorov scaling obtained at $t^* = 20$ and for (b) the compensated plot by multiplying the factor k^α, in which α is evaluated by the least square fitting in the range $2 \leq kl_K(t) \leq 5$.

to stress the behavior in the range $kl_K(t) > 1$. As shown in figure 3 (a), the normalized spectra almost collapse in the range $kl_K(t) < 1$, and they show the power-law decay for $kl_K(t) > 1$. The spectrum becomes less steep and approaches to k^{-2} with an increase of W_i, meaning that $E(k,t)$ is close to $E(k) \sim k^{-4}$. To see this point in more detail, we investigate the compensated spectra $k^\alpha E(k,t)$ plotted in figure 3 (b), where the exponent α is evaluated by the least square fit in the range $2 \leq kl_K(t) \leq 5$. This figure clearly indicates that 1) there is a clear scaling range for each curves of W_i, 2) the value of α decreases with an increase of W_i. The largest W_i case shows $\alpha = 4.14$ which is near the values of 3.5 and 3.8 obtained by the elastic turbulence [1, 6, 7].

The power-law form of $E(k,t)$ observed in figure 3 implies that the pressure spectrum $E_p(k,t)$ also obeys the power-law form. The pressure field $p(\boldsymbol{x},t)$ is determined by the NS equations with an incompressible condition as

$$p(\boldsymbol{x},t) = \Delta^{-1}\left(-\nabla\cdot(\boldsymbol{u}\cdot\nabla\boldsymbol{u}) + \nabla\cdot(\nabla : \boldsymbol{T}^p)\right). \tag{14}$$

When the turbulence adequately decays while the dumbbells remain the fully stretched configurations, the first term of the R.H.S. of Eq.(14) is sufficiently smaller than the second one, leading to the relationship $p(\boldsymbol{x},t) \simeq \Delta^{-1}\nabla\cdot(\nabla : \boldsymbol{T}^p)$ for $W_i \gg 1$ [9]. Thus the statistics of pressure field is dominated by that of the polymer stress field. Figure 4 shows the comparison of the pressure spectra $E_p(k,t) = 2\pi k^2\langle|\hat{p}(\boldsymbol{k},t)|^2\rangle_s$ obtained at $t^* = 20$ for all of the runs. The normalized plot by using the Kolmogorov scaling, shown in figure 4 (a), clearly represents that the pressure spectra obey the power-law form close to k^{-3} in the range $kl_K(t) > 1$. This is almost consistent with the experimental result by [9]. Spectra become less steep with an increase of W_i. This is confirmed by figure 4 (b) representing the compensated plot $k^\beta E_p(k,t)$ where the exponent β is also evaluated by the least square fitting in the range same as $E(k,t)$. We confirm the existence of plateaus in figure 4 (b) although there are some scatter of data when compared to the case of $k^\alpha E(k,t)$ (figure 3 (b)). The value of β decreases with an increase of W_i, where $\beta = 3.22, 3.02, 2.89$, and 2.78 for Runs D1,D2,D3, and D4. This feature is similar to the case for the kinetic energy spectrum (figure 3 (b)).

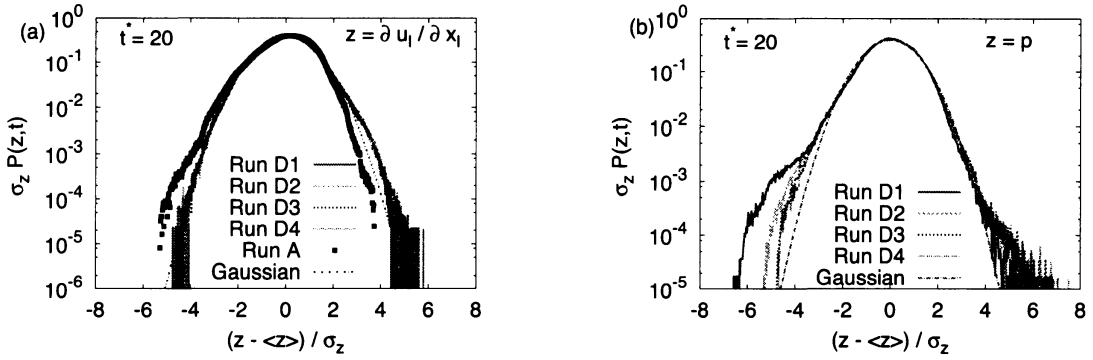

Figure 5: Comparison of the normalized PDFs for (a) longitudinal velocity derivative $\partial_L u_L$ and for (b) pressure p obtained at $t^* = 20$ for Runs D1, D2, D3 and D4.

Similarities of power-law spectra of both $E(k)$ and $E_p(k)$ between the present numerical results and the results by experimental observation suggest that the one-point statistics of the velocity derivative and pressure fields may show the strong non-Gaussianity [8, 9]. We further investigate the PDF behaviors for both the longitudinal velocity derivative field $\partial_L u_L(\boldsymbol{x}, t)$ and the pressure field $p(\boldsymbol{x}, t)$. Figure 5 shows the resulting curves obtained by the data at $t^* = 20$ for (a) $\partial_L u_L(\boldsymbol{x}, t)$ and (b) $p(\boldsymbol{x}, t)$, where we compare the curves made by the standardized plot. We confirm that the PDF form is almost insensitive to the variation of W_i for both cases, and slightly deviates from the Gaussian for $\partial_L u_L$. The PDF form of $\partial_L u_L$ by Runs D1-D4 becomes almost symmetric, meaning that the skewness factor of $\partial_L u_L$, which is related to the mean vorticity production in isotropic turbulence, is almost zero. This is in sharp contrast to the one-way coupling case (Run A), and is also consistent with the results of figure 2. While the curves for $p(\boldsymbol{x}, t)$ show almost Gaussian although the each curves are slightly skewed. Thus the velocity gradient and pressure field statistics manifest the less intermittent fluctuations than those by experimental results [8, 9], and are approximately Gaussian form. This suggests that the mechanism for producing the non-Gaussian statistics in experiments may not be attributed to the effects of polymers, perhaps is due to the nature of large-scale properties like the forcing mechanism. This calls further studies in the case for steady flow by introducing appropriate forcing mechanism. Also the PDF tail behavior is sensitive to the resolution condition [18], so that we may need further increase of spatial grid points to clarify the discrepancy between the present numerical and previous experimental results.

We discuss the power-law form of the spectra obtained in this study. Figure 3 (b) suggests that the scaling exponent α for the kinetic energy spectrum approaches to the value of 4 when W_i is increased further. The spectral form $E(k) \sim k^{-4}$ reminds us that of two-dimensional turbulence in the enstrophy inertial range, suggested by Saffman [19]. The key idea is the formation of the thin layer of vorticity field and leading to the large jump of vorticity, yields the power-law spectrum of vorticity spectrum $E_\omega(k) \sim k^{-2}$. Thus $E(k) \sim k^{-2} E_\omega(k) \sim k^{-4}$. This raises the question of how the field structure of vorticity field is characterized when $W_i \gg 1$. We expect to observe the large jump of vorticity, i.e. the regions having larger $|\nabla \boldsymbol{\omega}|$ localize in space. Figure 6 shows the iso-surface of $|\nabla \overline{\boldsymbol{\omega}}|$ obtained by Run D4 with $t^* = 20$, where we use the Gaussian filtered field $\overline{\hat{\boldsymbol{\omega}}}(\boldsymbol{k}) = \hat{\boldsymbol{\omega}}(\boldsymbol{k}) \exp\left(-(k/k_c)^2\right)$ to eliminate

Figure 6: Visualization of iso-surface of the absolute of vorticity derivative field $|\nabla\overline{\boldsymbol{\omega}}|$ obtained at $t^* = 20$ of Run D4.

the zig-zag fluctuations on the objects. This figure indicates that $|\nabla\overline{\boldsymbol{\omega}}|$ localizes in space as the sheet-like structures. This seems to support the idea by Saffman [19], although we do not know why such a sheet-like structure is formed due to the effect of polymers. Moreover we need further examinations by performing the simulations with larger W_i values than those by present study to confirm the asymptotic value of α when $W_i \to \infty$.

Finally we comment on the relationship between $E(k)$ and $E_p(k)$. In the final period of decay, the elastic energy for the ensemble of dumbbells is larger than the kinetic energy of fluid motion, as shown in figure 1. Also the mean enstrophy is produced by the polymer stress field rather than the vorticity stretching term originated from the advection term in the NS equations. These facts yield the evaluation of the order of velocity $\boldsymbol{u}$ and pressure p as $|\boldsymbol{u}| \sim (\nu/l)|\boldsymbol{T}^p|$, l being the characteristic scale in the scaling range, and $p \sim |\boldsymbol{T}^p|$ from Eq.(14) with $W_i \gg 1$. This estimation leads to the relationship $E(k) \sim (\nu k)^{-2} E_p(k)$, so that we have $\alpha - \beta = 2$. On the other hand, the numerical results by figures 3 and 4 indicate $\alpha - \beta = 1.38, 1.29, 1.30$, and 1.36 for Runs D1,D2,D3, and D4, being smaller than 2, although the values of $\alpha - \beta$ are insensitive to the variation of W_i. This means that the simple dimensional evaluation does not work well. We have no idea to explain this discrepancy at present, but this analysis suggests that the values of scaling exponent α and β are not simply extracted from the arguments by the dimensional grounds.

In summary, we investigated the scaling behavior of both the kinetic energy and pressure spectrum in decaying isotropic turbulence with polymer additives for various values of W_i for $W_i \gg 1$. We obtained the power-law forms of $E(k) \sim k^{-\alpha}$ and $E_p(k) \sim k^{-\beta}$ in the range $kl_K > 1$ when turbulence adequately decayed and the elastic energy became larger than the kinetic energy of fluid motions. Exponents α and β were approximately $4.2 - 4.6$ and $2.8 - 3.2$, and decreased with the increase in W_i. The value of β was similar to the values obtained in the recent experimental study of elastic turbulence ($\beta = 3$), while the value of α obtained by the largest value of W_i was slightly larger than those obtained by experiments ($\alpha = 3.5$) [1] and by the DNS of the constitutive equations ($\alpha = 3.8$) [6, 7]). Significant difference is observed in the PDF behavior of velocity derivative and pressure fields, where we observed the behavior close to the Gaussian irrespective of W_i, in contrast to the non-Gaussian statistics by experimental results [8, 9].

T. W. and T. G. were supported in part by Grants-in-Aid for Scientific Research Nos. 23760156 and 24360068, respectively, from the Ministry of Education, Culture, Sports, Sci-

ence, and Technology of Japan. T. W. would like to thank S. Uno and D. Sugimoto for their assistance in writing the parallelized code. The authors would like to thank the Theory and Computer Simulation Center of the National Institute for Fusion Science and JHPCN and HPC at the Information Technology Center of Nagoya University for providing the computational resources.

References

[1] A. Groisman and V. Steinberg, *Nature* **405**, 53–55, (2000)

[2] A. Groisman and V. Steinberg, *Nature* **410**, 905–908, (2001)

[3] T. Burghelea, E. Segre, and V. Steinberg, *Phys. Rev. Lett.* **92**, 164501 (2004).

[4] P. E. Arratia, C. C. Thomas, J. Diorio, and J. P. Gollub, *Phys. Rev. Lett.* **96**, 144502 (2006).

[5] T. Burghelea, E. Segre, and V. Steinberg, *Phys. Rev. Lett.* **96**, 214502 (2006).

[6] S. Berti, A. Bistagnino, G. Boffetta, A. Celani and S. Musacchio, *Phys. Rev. E* **77**, 055306 (2008).

[7] S. Berti and G. Boffetta, *Phys. Rev. E* **82**, 036314 (2010).

[8] A. Groisman and V. Steinberg, *New J. Phys.*, **6**, 29 (2004).

[9] Y. Jun and V. Steinberg, *Phys. Rev. Lett.* **102**, 124503 (2009).

[10] T. Watanabe and T. Gotoh, *J. Fluid. Mech.* **717**, 535 (2013).

[11] A. Fouxon and V. Lebedev, *Phys. Fluids* **15**, 2060 (2003).

[12] T. Watanabe and T. Gotoh, accepted for publication in *J. Phys.: Conf. Ser.*.

[13] R. B. Bird, C. F. Curtiss, R. C. Amstrong, and O. Hassager, *Dynamics of Polymetric Liquids, Vol.2 Kinetic Theory*, 2nd ed. (Wiley, New York, 1987).

[14] M. Doi and S. F. Edwards, *The Theory of Polymer Dynamics*, (Oxford University Press, New York, 1986).

[15] P. K. Yeung and S. B. Pope, *J. Comp. Phys.* **79**, 373–416 (1988).

[16] A. Prosperetti and G. Tryggvason (Eds.), *Computational Methods for Multiphase Flow*, (Cambridge University Press, Cambridge, 2007).

[17] T. Watanabe and T. Gotoh, *Phys. Rev. E* **81**, 066301 (2010).

[18] T. Watanabe and T. Gotoh, *J. Fluid Mech.* **590**, 117 (2007).

[19] P. G. Saffman, *Stud. Appl. Math.* **50**, 377 (1971).